International Symposium on Nonlinear Theory and its Applications
Xi'an, PRC, October 7–11, 2002

On the trade-off of ripple and spectral properties of chaotic dc-dc converters

A. L. Baranovski,** H. Güldner,* W. Schwarz,** J. Weber,* and O. Woywode*

Technische Universität Dresden, D-01062 Dresden, Germany
*Professur Leistungselektronik, **Professur Grundlagen der Elektrotechnik

Abstract

The paper analyzes a chaotic boost converter under peak current-mode control using slope compensation. Its embedded map of normalized inductor current samples is presented. Properties of the inductor current are expressed via the invariant density and moments of the map. The impact of slope compensation on the periodic and aperiodic operating range as well as the inductor current ripple is shown. The paper alludes to a method of calculating the inductor current's power density spectrum.

1. Introduction

Randomized or chaotic modulation schemes reduce the peaks of switching harmonics of switched mode dc-dc converters. Hence, they may meet electromagnetic interference (EMI) requirements with reduced EMI filter efforts [4]. One issue with random or chaotic operation is that the maximal time excursions of waveforms of the system's state variables increase [5].

Thus, random and chaotic operation may have superior spectral (frequency domain) but inferior ripple (time domain) performance with respect to periodic operation of dc-dc converters. The goal of this work is to find an optimized value of slope compensation that somewhat retains the periodic ripple properties while still benefiting from the spectral spreading of chaotic operation.

2. Boost converter and embedded map

Fig. 1 shows a current programmed mode (CPM) boost converter with stabilization ramp that provides slope compensation. Assuming that the voltage feedback loop guarantees a constant output voltage V_o, only the inner current loop is considered.

The active switch is closed until the inductor current $i(t)$ reaches the reference current

$$i_r(t) = I_r - c_r(t \bmod T) \tag{1}$$

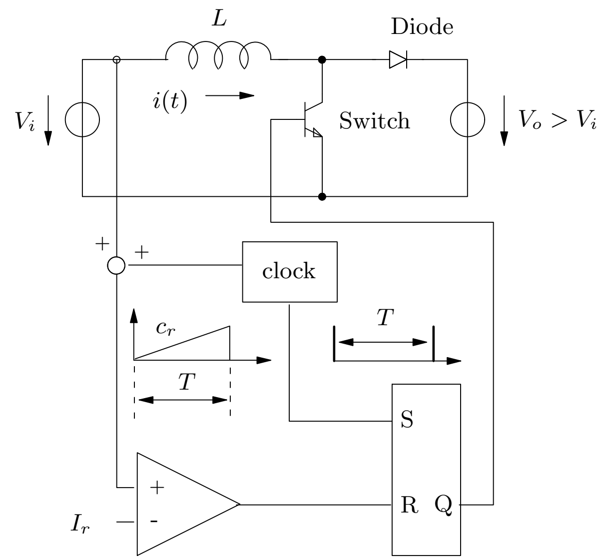

Figure 1: Open loop boost converter with slope compensation c_r, $V_i = 10\,\mathrm{V}$, $T = 100\,\mu\mathrm{s}$, $L = 1\,\mathrm{mH}$.

where c_r is the slope of the stabilization ramp[1]. The switch then opens and is closed until a clock impulse T arrives. Clock impulses arriving while the current ramps up are ignored. The converter is governed by

$$\mathrm{d}i/\mathrm{d}t = V_i/L = c_1 \quad \text{during } \textit{on} \text{ interval,} \tag{2}$$
$$\mathrm{d}i/\mathrm{d}t = (V_o - V_i)/L = c_2 \quad \text{during } \textit{off} \text{ interval,} \tag{3}$$

making up one switching cycle, with the *on* and *off* slopes, c_1 and c_2, respectively. For $c_2 > c_1$ or $V_o > 2V_i$ the converter exhibits chaotic behavior if no slope compensation is used. The stabilization ramp was traditionally used to enforce periodic operation for all voltage conversion ratios. Thereby the ramp restores a small ripple and improves the input ripple rejection of dc-dc converters. A small inductor current ripple leads to reduced output capacitor requirements, continuous conduction mode with light loads, and less output voltage

This work is supported by BMBF under FKZ 13N8134. Projektbetreuung durch VDI Physikalische Technologien.

[1]The slope may be added to the measured inductor current as shown in Fig. 1 or subtracted from I_r as suggested by (1).

ripple. These properties are poorly maintained during chaotic operation which motivates slope compensation. On the other hand, disadvantages may be attributed to the stabilization ramp, e. g. the ramp reduces the achievable output current [3].

Fig. 2 sketches the inductor current waveform with stabilization ramp. By inspection the inductor current

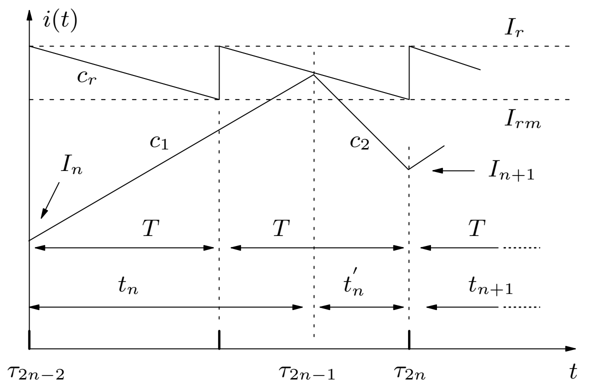

Figure 2: Chaotic waveform of inductor current.

can be expressed as

$$i(t) = \begin{cases} I_n + c_1\,(t - \tau_{2n-2}) & \tau_{2n-2} < t \leq \tau_{2n-1}, \\ i_r(\tau_{2n-1}) - c_2\,(t - \tau_{2n-1}) & \tau_{2n-1} < t \leq \tau_{2n}, \end{cases} \tag{4}$$

where the value of $i_r(\tau_{2n-1}) = I_n + c_1 t_n$ falls into the interval $[I_{rm}, I_r]$ and $I_{rm} = I_r - c_r T$ is the smallest value of the reference current. Note that the amount of slope compensation still allows for aperiodic waveforms.

From (2), (3), (4), and the pulse width modulation control scheme an explicit expression of subsequent inductor current samples $I_n = i(\tau_{2n-2})$ may be found. Normalized inductor current samples can then be expressed by a one-dimensional and piecewise linear map, $g : \mathbb{R} \to \mathbb{R}$, embedded in the boost converter shown in Fig. 1

$$y_{n+1} = g(y_n, \gamma) = \gamma(1 - y_n \bmod 1) \tag{5}$$

where

$$\begin{aligned} y_n &= (I_{rm} - I_n)/(c_1 T), \quad y_n \in [0, \gamma) && (6)\\ \gamma &= (\alpha - \beta)/(\beta + 1) > 0 \quad \text{as} \quad \alpha > \beta, && (7)\\ \alpha &= c_2/c_1 = V_o/V_i - 1 > 0 \quad \text{as} \quad V_o > V_i, && (8)\\ \beta &= c_r/c_1 > 0. && (9) \end{aligned}$$

γ is the bifurcation parameter. As indicated, $\gamma > 0$ because $c_2 > c_r$ in practical applications. A map of the form defined by (5) has already been found in [2, 4]. But there the bifurcation parameter is α which relates to the converter's voltage conversion ratio only. Now, γ depends not only on this ratio but also on the slope of the stabilization ramp. If $c_r = 0$, then $\gamma = \alpha$.

The duration of the *on* and *off* interval of any full switching cycle as well as the duration of the full switching cycle is given by

$$\begin{aligned} \frac{t_n}{T} &= y_n - \frac{\beta}{1+\beta}(y_n \bmod 1) + \frac{\beta}{1+\beta}, && (10)\\ \frac{t_n'}{T} &= 1 - \frac{1}{1+\beta}(y_n \bmod 1) - \frac{\beta}{1+\beta}, && (11)\\ \frac{t_n + t_n'}{T} &= 1 + \lfloor y_n \rfloor = \frac{\tau_{2n} - \tau_{2n-2}}{T}, && (12) \end{aligned}$$

respectively, as displayed in Fig. 2.

The Lyapunov exponent of map g is $\ln|\gamma|$ [2]. Hence, for $\gamma > 1$, CPM boost converters exhibit chaos which is consistent with the statement above. Fig. 3 shows

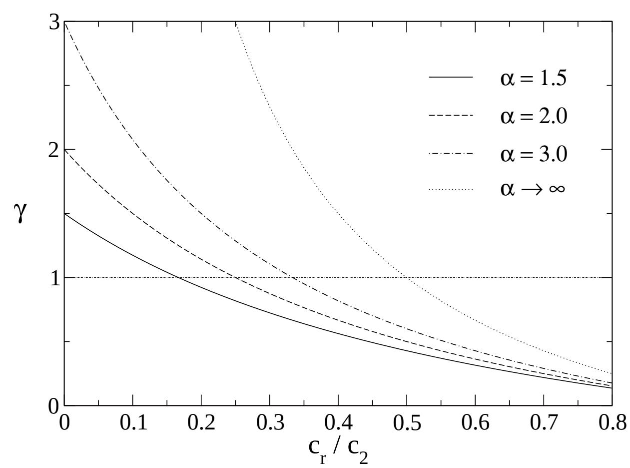

Figure 3: Impact of slope compensation

several curves γ versus the ratio c_r/c_2 with α as parameter and the line $\gamma = 1$ separates periodic and aperiodic behavior. Thus for a given voltage conversion ratio or α, Fig. 3 selects the appropriate slope compensation that yields periodic or aperiodic converter dynamics. The curve labeled $\alpha \to \infty$ shows that choosing $c_r = c_2/2$ guarantees periodic behavior for all voltage conversion ratios. This confirms a well known fact in power electronics for continuous inductor current topologies in CPM.

Fig. 3 picks up on the findings in [6]. There it was shown that large compensation to guarantee periodic behavior for a wide operating range compromises converter performance. Take the curve labeled $\alpha = 3$ in Fig. 3 as an example, choosing $c_r < c_2/2$ may still yield periodic behavior but allows for faster converter performance than $c_r = c_2/2$. The goal of this work is, however, to select a c_r that gives $\gamma > 1$ to benefit from reduced spectral peaks while maintaining a possibly small inductor current ripple.

3. Inductor current ripple

Map g is ergodic and possesses an invariant density $p(y,\gamma)$ on the interval $[0,\gamma)$. The evolution of this density is governed by the Frobenius-Perron-Operator (FPO). The invariant density determines the evolution of the inductor current samples via the respective map. Relevant properties of the inductor current may be calculated with respect to the invariant density. The properties are expressed using moments of the associated map. Moments of map g may be calculated according to [2]

$$m_k(\gamma) = E\left(y_n^k\right) = \int_0^\gamma y^k p(y,\gamma)\mathrm{d}y. \tag{13}$$

For integer γ, map g is fully stretching, the invariant density is uniform, and (13) becomes analytical $\gamma^k/(k+1)$ with $k = 1, 2, 3, \ldots$ while for non-integer γ it still gives an acceptable approximation. The approximation improves [7] if γ is larger than the golden mean $(1+\sqrt{5})/2$.

Let

$$\Delta i_n = i_r(\tau_{2n-1}) - I_n = c_1 t_n \tag{14}$$

define the peak-to-peak current ripple of the n$^{\text{th}}$ switching cycle where t_n follows from (10). The mean current ripple may be expressed through the first moment, using the integer approximation $m_1(\gamma) = \gamma/2$, of map g

$$E(\Delta i_n) = \frac{c_1 T}{1+\beta} \cdot \frac{\gamma - \beta\gamma + 3\beta}{2}. \tag{15}$$

The maximum current ripple is given by

$$\Delta i_{n,max} = c_1 T\alpha/(1+\beta) \tag{16}$$

Fig. 4 displays $\Delta i_{n,max}$ (solid line) normalized with respect to $c_1 T$. It further shows the numerical calculation of the mean inductor current ripple (dashed line) and its calculation using (15) (dotted line). Both curves are normalized to $c_1 T$ as well.

According to Fig. 4 the converter turns into periodic behavior at $\beta = 0.75$ which follows from inserting $\gamma = 1$ and $\alpha = 2.5$ in (7), and solving for β. Likewise, inserting $\gamma = (1+\sqrt{5})/2$ and $\alpha = 2.5$ in (7), solving again for β gives $\beta = (4-\sqrt{5})/(3+\sqrt{5})$, indicated by the vertical line in Fig. 4. This vertical line marks the region where (15) is almost as good as the numerical calculation of the mean inductor current ripple. Note further that more slope compensation to reduce the ripple hardly affects the mean current ripple.

Spectral spreading of the converter's strange attractor becomes significant if the strange attractor occupies the

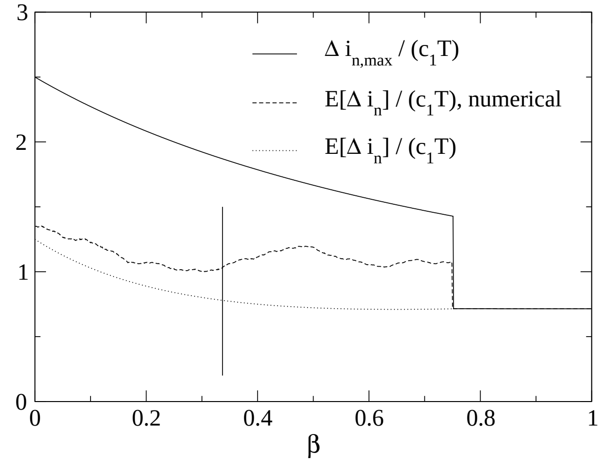

Figure 4: Normalized current ripples for $\alpha = 2.5$

entire state space. For map g, this happens at a specific value of the bifurcation paramter which coincides with the golden mean [7]. Fig. 4 indicates that slope compensation has a larger impact on the maximum than on the mean current ripple. Instead of having no slope compensation, i. e. $\beta = 0$, selecting β equal to $(4-\sqrt{5})/(3+\sqrt{5})$ reduces the maximum current ripple by about 25 %. The converter still exhibits chaotic behavior which may reduce the spectral peaks of the switching harmonics. At this point, the best compromise between ripple and spectral aspects seems to be a β somewhat below 0.337.

4. Power density spectrum

The second derivative of the inductor current yields an impulse process

$$y(t) = \frac{\mathrm{d}^2 i}{\mathrm{d}t^2} = c_1(\alpha+1)\sum_{n=0}^{\infty}(-1)^n\,\delta\left(t-\tau_n\right), \tag{17}$$

where the switching instants τ_n are given by

$$\tau_{2n} = t_n + t'_n + \tau_{2n-2}, \tag{18}$$

$$\tau_{2n+1} = \tau_{2n} + t_{n+1}. \tag{19}$$

The impulse process is illustrated in Fig. 5. For $\gamma > 1$ the sequence of delta functions is chaotic. Positive delta functions occur at even switching instants τ_n, i. e. they coincide with the multiples of the clock instants that cause the switch to close. These mulitples are generated by map g.

The power density spectrum (PDS) $S_i(\omega)$ of the inductor current is related to the PDS $S_y(\omega)$ of the chaotic impulse process in (17) by

$$S_i(\omega) = \frac{S_y(\omega)}{\omega^4}, \quad S_y(\omega) = \lim_{T^*\to\infty}\frac{\left|Y_{T^*}(\mathrm{j}\omega)\right|^2}{T^*} \tag{20}$$

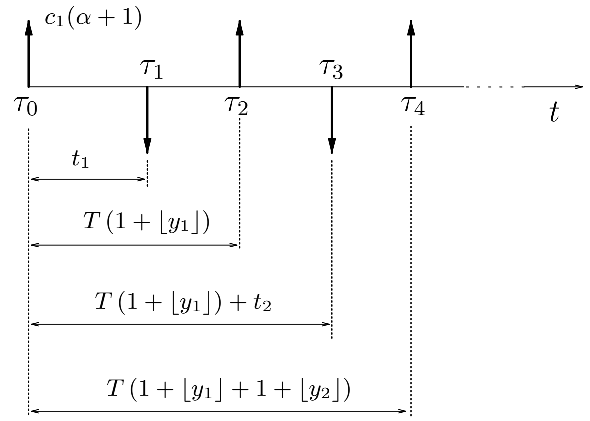

Figure 5: Impulse process associated with inductor current.

where $Y_{T^*}(\mathrm{j}\omega)$ is Fourier transform of one realization of $y(t)$ and T^* is the corresponding observation interval of one realization of this process. Following the method in [1] the PDS of $y(t)$ is

$$S_y(\omega) = \frac{2(c_1(1+\alpha))^2}{E(T_{si})} \sum_{k=-\infty}^{\infty} (-1)^k \Theta_{\tau_k}(\omega) \tag{21}$$

where the mean of the i$^{\text{th}}$ switching interval may be calculated via the first moment of map g

$$E(T_{si}) = T\int_0^{\gamma}(1+\lfloor y\rfloor)p(y,\gamma)\mathrm{d}x = T(1+1/\gamma)m_1(\gamma) \tag{22}$$

and $T^* \approx NE(T_{si})$ for large N.

$$\Theta_{\tau_k}(\omega) = E\left(\mathrm{e}^{\mathrm{j}\omega\tau_k}\right) = \int_{\Omega\tau_k} \mathrm{e}^{\mathrm{j}\omega\tau_k} \cdot p\left(\tau_k\right)\mathrm{d}\tau_k \tag{23}$$

are the characteristic functions, i. e. the Fourier transforms of the densities $p\left(\tau_k\right)$ of the cumulative sums of the chaotic *on* and *off* intervals. Referring to Fig. 5 a map between t_1 and t_2, i. e. between subsequent *on* intervals is rather complicated. This allows currently just brute force computation of the characteristic functions. We refrain from doing this at this point and need to postpone the calculation of the PDS.

5. Conclusion

This work analyzed a CPM boost converter that employs slope compensation. The traditional purpose of the stabilization ramp may be redefined. The ramp no longer needs to avoid chaotic inductor current waveforms but may be selected to meet a desired PDS (provided an explicit expression can be found) and current ripple. The benefit of the chaotic inductor current is a spread spectrum (measured by the PDS of the inductor current) that may allow for smaller EMI filters. To really tailor ripple and spectrum analytical expressions for the characteristic functions need to found.

References

[1] A. L. Baranovski, A. Mögel, and W. Schwarz. Chaotic pulse processes - spectral analysis and signal generation. In *Workshop on Nonlinear Dynamics of Electronic Systems, NDES 1999*, pages 69–72, Rønne, Bornholm, Denmark, July 1999.

[2] A. L. Baranovski, A. Mögel, W. Schwarz, and O. Woywode. Statistical analysis of a dc-dc converter. In *Workshop on Nonlinear Dynamics of Electronic Systems Rec., NDES 1999*, pages 77–80, Rønne, Bornholm, Denmark, July 1999.

[3] J.-H. Cheng and A. F. Witulski. Steady-state and large-signal design of current programmed dc-dc converters. *IEEE Trans. Power Electronics*, 12(4):743–751, July 1997.

[4] J. H. B. Deane, P. Ashwin, D. C. Hamill, and D. J. Jefferies. Calculation of the periodic spectral components in a chaotic dc-dc converter. *IEEE Trans. Circuits and Systems—I: Fundamental Theory and Applications*, 46(11):1313–1319, November 1999.

[5] A. M. Stanković, G. C. Verghese, and D. J. Perreault. Analysis and synthesis of randomized modulation schemes for power converter. *IEEE Trans. Power Electronics*, 10(6):680–693, November 1995.

[6] C. K. Tse and Y. M. Lai. Control of bifurcation in current-programmed dc/dc converters: A reexamination of slope compensation. In *IEEE International Symposium on Circuits and Systems Rec., ISCAS 2000*, pages I–671–I–674, Geneva, Switzerland, May 2000.

[7] O. Woywode, J. Weber, and H. Güldner. A topological and statistical approach to dc-dc converters. In *Power Electronics Specialists' Conference Rec., PESC 2001*, pages 439–444, Vancouver, Canada, June 2001.